RSC Advances

PAPER

View Article Online
View Journal | View Issue

Cite this: *RSC Adv.*, 2025, **15**, 14739

Au nanoparticles with oxygen vacancies on $BiVO_4$ for electrocatalytic nitrate reduction to ammonia†

Kui Hu,[a] Shengbo Zhang, *[bc] Zhixian Mao,[bc] Dongnan Zhao,[b] Daopeng Li,[bc] Zhongjun Li, [a] Qiang Li,[a] Qiong Tang*[a] and Tongfei Shi*[bc]

Received 6th February 2025
Accepted 14th April 2025

DOI: 10.1039/d5ra00886g

rsc.li/rsc-advances

Ammonia (NH_3) is an important energy carrier and agricultural fertilizer. Development of electrocatalysts for efficient NH_3 electrosynthesis *via* the nitrate reduction reaction (NitRR) is highly desirable but remains a key challenge. In this work, we successfully loaded Au nanoparticles on $BiVO_4$ by a one-step hydrothermal method. It is demonstrated that by using Au nanoparticles (10–15 nm) embedded on $BiVO_4$ (Au/$BiVO_4$) with oxygen vacancies (Au loading is 1.3 wt%), the electrocatalytic NitRR is indeed possible under ambient conditions. Unexpectedly, at −1.35 V (*vs.* RHE), the yield rate for NH_3 of Au/$BiVO_4$ reached 3320.9 ± 89.9 μg h^{-1} cm^{-2}, which was far superior to (11.3 μg h^{-1} cm^{-2}) pristine $BiVO_4$. The ^{15}N isotope labeling experiments confirmed that the produced NH_3 indeed originated from the nitrate reduction reaction catalyzed by Au/$BiVO_4$. The comprehensive analysis further confirms that the oxygen vacancies in Au/$BiVO_4$ can effectively weaken the N–O bonding and restrain the formation of by-products, resulting in high faradaic efficiency and NH_3 selectivity. Furthermore, *in situ* differential electrochemical mass spectrometry (DEMS) was adopted to monitor the electrochemical separation of the NitRR products on the surface of Au/$BiVO_4$.

Ammonia (NH_3) has attracted considerable interest as a sustainable nitrogen fertilizer in its anhydrous and salt forms, as well as a viable alternative fuel for transportation and an efficient hydrogen energy carrier.[1–3] Currently, ammonia synthesis remains predominantly dependent on the energy- and capital-intensive Haber-Bosch process (150–350 atm, 350–550 °C), in which hydrogen and energy inputs are primarily sourced from fossil fuels, leading to substantial CO_2 emissions.[4–7] With the depletion of fossil fuel reserves and escalating concerns over greenhouse gas emissions, the development of more sustainable and cost-effective ammonia production technologies is imperative to meet the increasing global demand. In recent years, electrocatalytic and photo(electro)catalytic conversion of nitrogen gas and water into ammonia under ambient conditions has garnered significant attention.[8–11] However, the faradaic efficiency (FE) remains severely constrained by the high dissociation energy of the N≡N bond (941 kJ mol^{-1}), the limited solubility of nitrogen gas in electrolytes, and the competing hydrogen evolution reaction (HER).[7,12,13] Thus, developing a new route for ammonia synthesis under benign conditions is urgently desired. Given that the N–O bond dissociation energy in nitrate is relatively low (204 kJ mol^{-1}) and ammonia can be readily recovered from aqueous solutions, utilizing nitrate contaminants as a nitrogen source and water as a hydrogen source for the electrochemical synthesis of value-added NH_3 has attracted considerable interest.[14–16] However, the competing hydrogen evolution reaction (HER) and the inherently complex eight-electron transfer process significantly limit the faradaic efficiency (FE) and selectivity of NH_3 in electrocatalytic nitrate reduction reactions (NitRR).[17–19] Therefore, the rational design and precise engineering of high-performance electrocatalysts are essential to overcoming these challenges.

Theoretical studies have demonstrated that oxygen vacancies (OVs) exhibit unique electronic modulation functions in catalytic reactions. By optimizing the adsorption energy of reaction intermediates and lowering the activation barrier, thereby significantly promoting reaction pathways toward lower energy consumption.[20] Surface characterization and theoretical calculations have confirmed that NO_x molecules can be effectively activated into highly reactive intermediate states under different coverage conditions and adsorption configurations.[21] By precisely constructing electron-donating semiconductor catalytic systems enriched with oxygen vacancies, it is possible not only to overcome the kinetic limitations of conventional nitrogen oxide reduction reactions but also to enhance surface adsorption strength and electron transfer efficiency, thereby

[a]*School of Physics, Hefei University of Technology, Hefei 230009, Anhui, China. E-mail: jennytq@hfut.edu.cn*

[b]*Key Laboratory of Materials Physics, Centre for Environmental and Energy Nanomaterials, Anhui Key Laboratory of Nanomaterials and Nanotechnology, CAS Center for Excellence in Nanoscience Institute of Solid State Physics, HFIPS, Chinese Academy of Sciences, Hefei 230031, China. E-mail: tfshi@issp.ac.cn; shbzhang@issp.ac.cn*

[c]*University of Science and Technology of China, Hefei 230026, China*

† Electronic supplementary information (ESI) available. See DOI: https://doi.org/10.1039/d5ra00886g

significantly improving the catalytic activity for nitrogen oxide reduction. Recently, oxygen vacancies (OVs) have been widely used to improve the performance of electrocatalysts. For example, Zeng and co-workers demonstrated that $LaCoO_3$ with OVs is proposed for efficient electrocatalytic NRR.[22] Density functional theory calculations revealed that enhanced activation of N_2 over V_o-$LaCoO_3$ originated from the increased charge density around the valence band edge *via* the introduction of OVs.[22] Moreover, Zhang *et al.* reported the TiO_2 nanotubes with rich oxygen vacancies that exhibited enhanced high FE (85.0%) and selectivity (87.1%) toward the NH_3 synthesis from nitrate electroreduction.[23] Theoretical calculations combined with *in situ* measurements reveal that the oxygen atoms in nitrate can occupy the oxygen vacancies in TiO_{2-x}, thereby weakening the N–O bond. Furthermore, a higher concentration of oxygen vacancies enhances NH_3 selectivity by modulating the interaction between intermediates and the catalyst.[23]

Therefore, combined with the theoretical calculations with experimental observations, we have designed and constructed the Au nanoparticles embedded on $BiVO_4$ (Au/$BiVO_4$) with oxygen vacancies through a facile and controllable strategy. And the as-prepared Au/$BiVO_4$ exhibits brilliant NitRR performances, including high NH_3 yield rate of 3320.9 ± 89.9 μg h^{-1} cm^{-2}, high FE (up to 59.6 ± 2.4%) at −1.35 V (*vs.* RHE), and good stability (up to 10 h). The enhanced NitRR electrocatalytic activities mainly originate from the enhanced nitrate adsorption energy and a more favorable active reaction site due to the introduction of OVs in Au/$BiVO_4$, which can effectively weaken the N–O bonding and restrain the formation of by-products, resulting in high faradaic efficiency and NH_3 selectivity.

The Au nanoparticles (NPs) prepared by reducing $HAuCl_4 \cdot 4H_2O$ with $NaBH_4$ were loaded into $BiVO_4$ to form Au/$BiVO_4$ as shown in Fig. 1a. The transmission electron microscopy (TEM) image of Au/$BiVO_4$ shows that $BiVO_4$ has a fusi form structure, Au NPs are uniformly distributed on the surface of the $BiVO_4$ support (Fig. 1b). Furthermore, the well-resolved lattice fringes of 0.246 nm in High-resolution transmission electron microscopy (HR-TEM) image of Au/$BiVO_4$ corresponded to the (111) plane of cubic Au phase,[24,25] demonstrated the successful deposition of Au NPs on $BiVO_4$ surface (Fig. 1c). X-ray diffraction (XRD) was used to analyse the crystal structure of the as-prepared Au/$BiVO_4$ sample. As shown in Fig. 1d, the present XRD pattern of Au/$BiVO_4$ has three strong diffraction peaks at 30.7°, 32.9°, and 48.6°, corresponding to (211), (112), and (312) crystal planes of $BiVO_4$ (PDF No. 14-0688).[26] The diffraction peaks located at 38.2° belong to the (111) crystal planes of Au (PDF No. 04-0784),[27] which is in good agreement with the HR-TEM results. However, due to the low gold content, the intensity of the diffraction peaks is not strong. Moreover, the corresponding element mapping images displayed that Au NPs was uniformly distributed on $BiVO_4$ (Fig. 1e). The loading content of Au NPs in Au/$BiVO_4$ is 1.3 wt% from Fig. S1 (ESI†), corresponding to the weak diffraction peak in XRD pattern. The pore size distribution of Au/$BiVO_4$ demonstrates its micro- and mesoporous structure (Fig. 1f), which allows for the exposure of more active sites are beneficial for the transport of electrons and the mass transport of electrolytes during electrolysis.[28]

X-ray photoelectron spectroscopy (XPS) was employed to investigate the chemical composition and valence state variations of the catalyst, providing further insights into the electronic interactions between Au NPs and $BiVO_4$. The survey spectra in Fig. S2 (ESI†) exhibit distinct peaks corresponding to Bi, Au, V, and O, indicating that these elements are the primary constituents of the catalyst, which is consistent with the element mapping characterization. The high-resolution Au 4f spectrum (Fig. 2a) contains two predominant peaks at 83.9 eV and 87.5 eV indicate the successful formation of Au.[29] In the XPS spectra of Bi 4f spectra (Fig. 2b), two distinctive peaks corresponded to Bi $4f_{7/2}$ in pristine $BiVO_4$ are observed at 158.7 eV and 160.0 eV, respectively, while the Bi $4f_{7/2}$ in Au/$BiVO_4$ has only one characteristic peak at 159.1 eV.[30] For the O 1s XPS

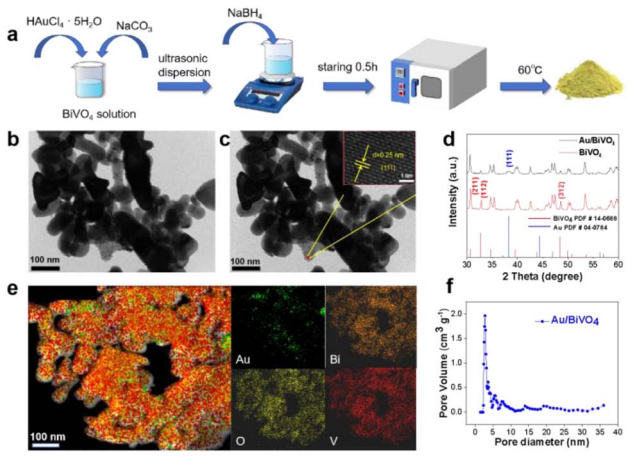

Fig. 1 (a) Schematic for diagram illustrating synthetic procedure of Au/$BiVO_4$. (b) TEM and (c) HR-TEM images of Au/$BiVO_4$. (d) XRD pattern of Au/$BiVO_4$. (e) HAADF-STEM and corresponding elemental mapping images of Au/$BiVO_4$. (f) Pore size distribution curve of Au/$BiVO_4$.

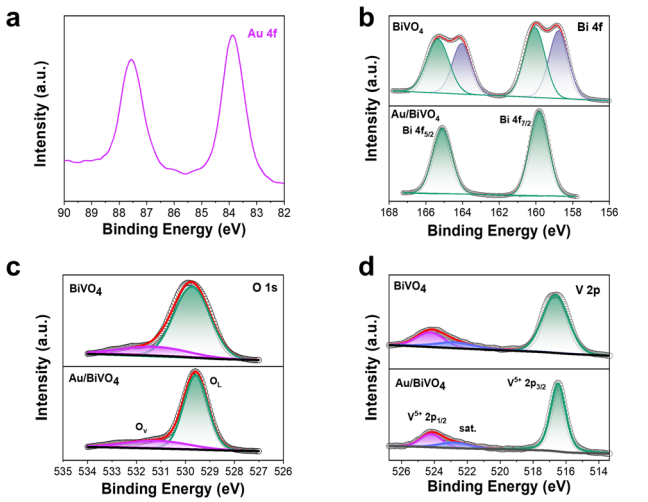

Fig. 2 High-resolution XPS spectra of (a) Au 4f, (b) Bi 4f, (c) O 1s, (d) V 2p and of pristine $BiVO_4$ and Au/$BiVO_4$.

spectra in Fig. 2c, where two peaks at 529.7 eV and 531.3 eV correspond to lattice oxygen and oxygen vacancy in pristine $BiVO_4$, respectively. Compared to pristine $BiVO_4$, the O 1s binding energies of the lattice oxygen and oxygen vacancy peaks of the Au/$BiVO_4$ were reduced by 0.1 eV. Studies have demonstrated that under high-temperature and reducing conditions, lattice oxygen atoms are prone to detachment, leading to the formation of oxygen vacancies. Moreover, the strong reducing agent $NaBH_4$ can further induce the removal of oxygen atoms from the $BiVO_4$ crystal lattice, contributing to the generation of additional oxygen vacancies.[31,32] In the V^{5+} 2p spectra (Fig. 2d), the peaks of V^{5+} in Au/$BiVO_4$ located at 516.6 eV and 524.3 eV show a slight low-energy shift in contrast to pristine $BiVO_4$, indicates that V species in $BiVO_4$ are stable after loading Au. More importantly, the related changes in the valence state further demonstrate that the charge transferred from $BiVO_4$ to Au NPs. The induced local charge redistribution contributes to the targeted adsorption of reactant species and thus enhances the electrocatalytic NitRR to NH_3 production ability.[33]

The NitRR performance of the catalyst was evaluated using a three-electrode H-type electrolytic cell. Initial voltammetric verification of NitRR on Au/$BiVO_4$ was carried out by linear sweep voltammetry (LSV). Fig. 3a shows the LSV curves of the catalyst in electrolytes of 0.1 M K_2SO_4 and 0.1 M K_2SO_4 + 0.1 M KNO_3. Compared with the LSV curve for 0.1 M K_2SO_4, the current density was markedly enhanced following the introduction of KNO_3, indicating a strong reduction reaction at the cathode after the addition of nitrate. By analyzing the two LSV curves, we chose to perform the NitRR at 0.05 V intervals within the applied potential range of −1.1 V to−1.35 V (*vs.* RHE). The obtained current density curves and corresponding UV-vis absorption spectra are shown in Fig. S3 (ESI†) and the produced NH_3 was determined by the indophenol blue method (Fig. S4, ESI†). Fig. 3b shows the R_{NH_3} and FE at different applied potentials. It can be observed that as the negative potential increases, the R_{NH3} increases from 1385.5 ± 158.0 μg h^{-1} cm^{-2} at −1.1 V (*vs.* RHE) to a maximum of 3320.9 ± 89.9 μg h^{-1} cm^{-2} at −1.35 V (*vs.* RHE) with an FE of 59.6 ± 2.4%. The results demonstrate that the Au/$BiVO_4$ catalyst has a good performance towards the NitRR to NH_3. Except for the NH_3 main product, the by-product NO_2^- was also detected in the electrolyte (Fig. S5, ESI†).

A series of controlled experiments were conducted to eliminate the influence of other factors on NH_3 production (Fig. 3c, ESI†). Firstly, the NitRR was carried out using Au/$BiVO_4$ catalyst in electrolyte of 0.1 M K_2SO_4 at −1.35 V (*vs.* RHE). The results demonstrate that there is a negligible quantity of ammonia produced. Furthermore, the presence of ammonia was not discernible when the electrolyte was 0.1 M K_2SO_4 + 0.1 M KNO_3 but without applied potential (OCP). The above experiment eliminated the effect of environmental factors on ammonia production. In order to eliminate any potential interference from carbon paper, pure carbon paper was employed in the NitRR process. The lower R_{NH_3} and FE can infer that the excellent ammonia production activity is mainly attributed to the prepared Au/$BiVO_4$ catalyst. Moreover, to investigate the effect of the interaction between Au and $BiVO_4$ on the catalysis of NitRR to ammonia, $BiVO_4$ was used as the working electrode under 0.1 M K_2SO_4 and 0.1 M KNO_3 for 2 h at −1.35 V (*vs.* RHE). Only negligible NH_3 concentration was detected. This demonstrates that addition of Au nanoparticles can facilitate the generation and stabilization of oxygen vacancies, while these vacancies, in turn, anchor the Au nanoparticles and optimize their electronic structure, significantly enhancing electron transfer efficiency. This synergistic interaction effectively boosts the catalytic activity and selectivity for NO_3^- reduction, thereby enabling high-efficiency and stable catalytic performance.[34,35] To investigate the synergistic effect of gold loading on oxygen vacancy concentration and the electrochemical probe reaction performance of the composites, we optimized the Au-to-oxygen vacancy ratio by adjusting the Au loading. Fig. S6† is the R_{NH_3} and FE of catalyst at different Au loading during a 2 h NitRR measurement. It can be observed that Au/$BiVO_4$ exhibits superior performance, suggesting that, at this specific loading, the oxygen vacancy concentration on the catalyst surface achieves an optimal balance with the distribution of active sites. To further verify the source of NH_3, $K^{15}NO_3$ was used instead of $K^{14}NO_3$ for the NitRR, and the resulting products were qualitatively analyzed for NH_3 yield using ^1H nuclear magnetic resonance (NMR) spectra. The results indicate that the ^1H NMR spectrum of the electrolyte containing $^{15}NO_3^-$ as the reactant exhibits the characteristic doublet of $^{15}NH_4^+$(Fig. 3d). This result reveals that the produced NH_3 is completely derived from nitrate. Besides superior activity, the stability of the catalyst is another crucial parameter for practical applications. Cyclic

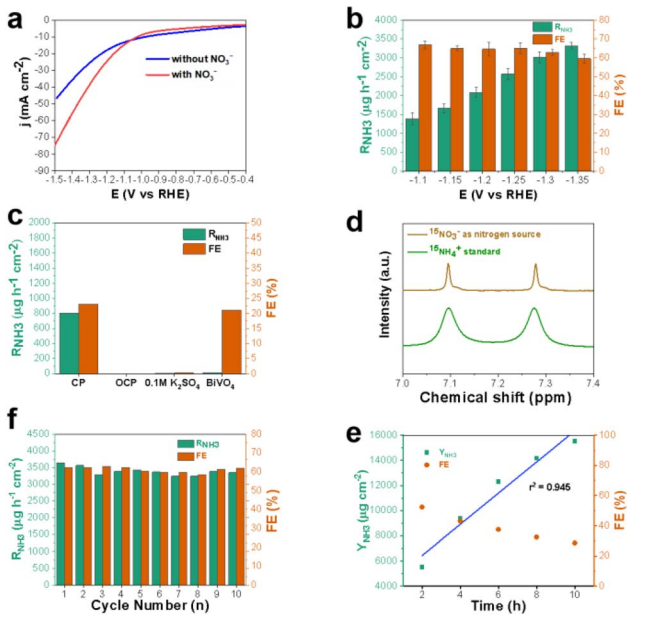

Fig. 3 (a) LSV curves of Au/$BiVO_4$ catalyst in 0.1 M K_2SO_4 and 0.1 M K_2SO_4 + 0.1 M KNO_3 solution. (b) R_{NH_3} and FE of Au/$BiVO_4$ catalyst obtained at different potentials for 2 h NitRR measurement. (c) Comparison of R_{NH_3} and FE under different conditions. (d) ^1H NMR spectra of Au/$BiVO_4$ catalyst using $^{15}NO_3^-$ as nitrogen source for NitRR and standards $(^{15}NH_4)_2SO_4$. (f) Recycling tests for Au/$BiVO_4$ catalyst during NitRR at −1.35 V (*vs.* RHE). (e) The FE and NH_3 yield were monitored over a 10 h NitRR conducted at −1.35 V (*vs.* RHE).

stability of the electrocatalyst is an important factor for practical application. For the evaluation of the cyclic stability of Au/$BiVO_4$, the consecutive NitRR test was performed for 10 times at −1.35 V (*vs.* RHE). The R_{NH3} and FE of the Au/$BiVO_4$ have no obvious change after 10 consecutive electrolysis cycles (Fig. 3f). The sustainability of the catalyst was further tested by reacting at −1.35 V (*vs.* RHE) for 10 h (Fig. S7, ESI†). It can be seen that throughout the experiment, the NH_3 yielded increases linearly with time and the FE decreases uniformly (Fig. 3e). This phenomenon can be attributed to the accumulation of reaction by-products on the electrode surface, which impedes the accessibility of reactants to active sites, consequently resulting in a reduction in the FE of the reaction. This indicates that the Au/$BiVO_4$ catalyst has good stability. To determine the structural stability, careful examination of XPS characterization on Au/$BiVO_4$ after NitRR test (Fig. S8, ESI†) confirms the high structural stability of Au/$BiVO_4$. To evaluate the scalability of the catalyst for potential large-scale applications, we systematically assessed the performance of Au/$BiVO_4$ by constructing an expanded reaction system (50 mL–100 mL) and gradually increasing the nitrate concentration (0.1 M–0.2 M). Fig. S9† presents the R_{NH_3} and FE of Au/$BiVO_4$ at different scales. In the 100 mL electrolysis system, the catalyst retained its catalytic activity comparable to that in the smaller-scale system, demonstrating excellent scalability. When the nitrate concentration was increased to 0.2 M, the R_{NH_3} was enhanced compared to that at 0.1 M, revealing a significant mass transfer enhancement effect. These findings strongly validate the feasibility of this catalyst for large-scale applications.

Furthermore, the *in situ* differential electrochemical mass spectrometry (DEMS) is employed for *in situ* detection of molecular intermediate and product over Au/$BiVO_4$.[36] The gaseous molecules can be identified based on *m*/*z* values, and the relative quantities of intermediates and products can be estimated in real-time based on signal intensity.[37] In order to investigate the electrocatalytic NitRR pathway throughout the system, *in situ* electrochemical differential mass spectrometer (DEMS) was employed for the detection of intermediates and reduction products. During the electrocatalytic experiments, reaction products and intermediates were transported to the online mass spectrometry analysis system *via* a vacuum pump for real-time monitoring and analysis based on mass-to-charge ratio (*m*/*z*). The signal intensity enables analysis of the real-time concentration of intermediates and products. As shown in Fig. 4, the signal peaks at *m*/*z* 17, 30, 31, 32, 33 and 46 clearly indicate the presence of $*NH_3$, *NO, *HNO, $*NH_2O$, $*NH_2OH$ and $*NO_2$ intermediates during the reaction. Based on these results, the electrocatalytic NitRR pathway on Au/$BiVO_4$ catalyst is proposed to be the following: $NO_3^- \rightarrow *NO_3 \rightarrow *NO_2 \rightarrow *NO \rightarrow *NHO \rightarrow *NH_2O \rightarrow *NH_2OH \rightarrow *NH_3 \rightarrow NH_3$ (g).

In summary, Au nanoparticles embedded on $BiVO_4$ (Au/$BiVO_4$) with oxygen vacancies (OVs) have been successfully synthesized through a facile and controllable strategy. Owing to the enhanced NO_3^- adsorption energy and a more favourable active reaction site at the OVs due to the introduction of Au NPs to $BiVO_4$. The as-synthesized Au/$BiVO_4$ catalyst exhibits superior NitRR performances, including high NH_3 yield rate of 3320.9 ± 89.9 μg h^{-1} cm^{-2} and high FE of 59.6 ± 2.4% at −1.35 V (*vs.* RHE), and good stability (up to 10 h) at room temperature and atmospheric pressure. This work is not only the excellent report on noble metal NitRR electrocatalyst achieving both high NH_3 yield rate and high FE imultaneously, but also opens up a new avenue for exploring the practical applications of the transition metal vanadium oxides and vanadates family as very attractive low-cost NitRR electrocatalysts.

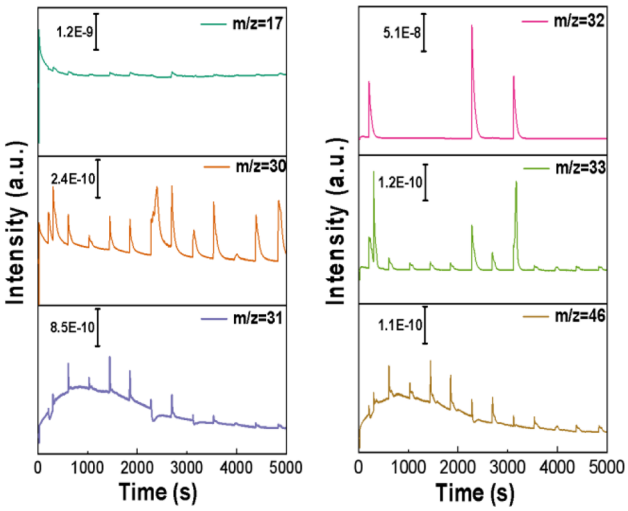

Fig. 4 *In situ* DEMS measurements of NitRR over Au/$BiVO_4$.

Data availability

The data supporting this article have been included as part of the ESI.†

Author contributions

Kui Hu: conceptualization, investigation, visualization, writing – original draft. Shengbo Zhang: data curation, resources, supervision, writing – review & editing. Zhixian Mao: investigation, resources, formal analysis. Dongnan Zhao: investigation, resources, formal analysis. Daopeng Li: investigation, resources, formal analysis. Zhongjun Li: software. Qiang Li: software. Qiong Tang: data curation, resources, supervision. Tongfei Shi: funding acquisition, supervision, resources, writing – review & editing.

Conflicts of interest

There are no conflicts to declare.

Acknowledgements

This work was financially supported by the Natural Science Foundation of Anhui Provincial Natural Science Foundation (Grant No. 2408085MB021).

Notes and references

1 Y. Xu, Y. W. Sheng, M. Z. Wang, T. T. Liu, H. J. Yu, K. Deng, Z. Q. Wang, L. Wang and H. J. Wang, Lattice-strain and Lewis acid sites synergistically promoted nitrate electroreduction to ammonia over PdBP nanothorn arrays, *J. Mater. Chem. A*, 2022, **10**(30), 16290–16296.

2 A. J. Ma, J. Z. Gui, Y. M. Huang and Y. F. Yu, Electrocatalytic coupling of anodic nitrogen oxidation and cathodic nitrate reduction for ammonia synthesis from air and water, *Nano Res.*, 2024, **17**(9), 7824–7829.

3 X. Fan, C. Liu, Z. Li, Z. Cai, L. Ouyang, Z. Li, X. He, Y. Luo, D. Zheng and S. J. S. Sun, Pd-Doped Co_3O_4 nanoarray for efficient eight-electron nitrate electrocatalytic reduction to ammonia synthesis, *Small*, 2023, **19**(42), 2303424.

4 S. Ghavam, M. Vahdati, I. A. G. Wilson and P. Styring, Sustainable Ammonia Production Processes, *Front. Energy Res.*, 2021, **9**, 19.

5 M. van Kessel, D. R. Speth, M. Albertsen, P. H. Nielsen, H. J. M. Op den Camp, B. Kartal, M. S. M. Jetten and S. Lücker, Complete nitrification by a single microorganism, *Nature*, 2015, **528**(7583), 555–559.

6 J. Wang, T. Feng, J. X. Chen, V. Ramalingam, Z. X. Li, D. M. Kabtamu, J. H. He and X. S. Fang, Electrocatalytic nitrate/nitrite reduction to ammonia synthesis using metal nanocatalysts and bio-inspired metalloenzymes, *Nano Energy*, 2021, **86**, 106088.

7 L. Q. Li, C. Tang, B. Q. Xia, H. Y. Jin, Y. Zheng and S. Z. Qiao, Two-Dimensional Mosaic Bismuth Nanosheets for Highly Selective Ambient Electrocatalytic Nitrogen Reduction, *ACS Catal.*, 2019, **9**(4), 2902–2908.

8 X. L. Xue, R. P. Chen, C. Z. Yan, P. Y. Zhao, Y. Hu, W. J. Zhang, S. Y. Yang and Z. Jin, Review on photocatalytic and electrocatalytic artificial nitrogen fixation for ammonia synthesis at mild conditions: advances, challenges and perspectives, *Nano Res.*, 2019, **12**(6), 1229–1249.

9 A. B. Silva, E. A. Reis, J. Hu, J. Albero, C. Ribeiro, L. H. Mascaro and H. García, Improving nitrate-to-ammonia conversion efficiency on electrodeposited nickel phosphide *via* surface *δ*-FeOOH modification, *J. Mater. Chem. A*, 2025, **13**(6), 4576–4586.

10 G. R. Xu, H. Li, A. S. R. Bati, M. Bat-Erdene, M. J. Nine, D. Losic, Y. Chen, J. G. Shapter, M. Batmunkh and T. Y. Ma, Nitrogen-doped phosphorene for electrocatalytic ammonia synthesis, *J. Mater. Chem. A*, 2020, **8**(31), 15875–15883.

11 Y. Liu, Y. Su, X. Quan, X. Fan, S. Chen, H. Yu, H. Zhao, Y. Zhang and J. J. A. C. Zhao, Facile ammonia synthesis from electrocatalytic N_2 reduction under ambient conditions on N-doped porous carbon, *ACS Catal.*, 2018, **8**(2), 1186–1191.

12 Y. Cui, A. Dong, Y. Zhou, Y. Qu, M. Zhao, Z. Wang and Q. J. S. Jiang, Interfacially engineered nanoporous Cu/MnO_x hybrids for highly efficient electrochemical ammonia synthesis *via* nitrate reduction, *Small*, 2023, **19**(17), 2207661.

13 Y. J. Yang, S. Q. Wang, H. M. Wen, T. Ye, J. Chen, C. P. Li and M. Du, Nanoporous Gold Embedded ZIF Composite for Enhanced Electrochemical Nitrogen Fixation, *Angew. Chem., Int. Ed.*, 2019, **58**(43), 15362–15366.

14 J. Martínez, A. Ortiz and I. Ortiz, State-of-the-art and perspectives of the catalytic and electrocatalytic reduction of aqueous nitrates, *Appl. Catal., B*, 2017, **207**, 42–59.

15 Y. H. Cui, C. N. Sun, G. P. Ding, M. Zhao, X. Ge, W. Zhang, Y. F. Zhu, Z. L. Wang and Q. Jiang, Synergistically tuning intermediate adsorption and promoting water dissociation to facilitate electrocatalytic nitrate reduction to ammonia over nanoporous Ru-doped Cu catalyst, *Sci. China Mater.*, 2023, **66**(11), 4387–4395.

16 D. X. Liu, Z. Meng, Y. F. Zhu, X. F. Sun, X. Deng, M. M. Shi, Q. Hao, X. Kang, T. Y. Dai, H. X. Zhong, J. M. Yan and Q. Jiang, Gram-level NH_3 Electrosynthesis *via* NO_x reduction on a Cu Activated Co Electrode, *Angew. Chem., Int. Ed.*, 2024, **136**(1), e202315238.

17 Y. Xu, K. K. Shi, T. L. Ren, H. J. Yu, K. Deng, X. Wang, Z. Q. Wang, H. J. Wang and L. Wang, Electronic Metal-Support Interaction Triggering Interfacial Charge Polarization over CuPd/N-Doped-C Nanohybrids Drives Selectively Electrocatalytic Conversion of Nitrate to Ammonia, *Small*, 2022, **18**(42), 10.

18 S. Chen, F. Yin, X. He and J. J. C. Tan, The Preparation of UiO-66-NH_2/CNT Electrocatalyst and its High Catalytic Performance for Electrochemical Synthetic Ammonia in Neutral Electrolyte, *ChemistrySelect*, 2023, **8**(9), e202204988.

19 J. Li, R. Valenza and S. J. S. Haussener, In Situ Synthesis of Cu_xO/N Doped Graphdiyne with Pyridine N Configuration for Ammonia Production *via* Nitrate Reduction, *Small*, 2024, **20**(33), 2310467.

20 J. Li, H. Li, G. M. Zhan and L. Z. Zhang, Solar Water Splitting and Nitrogen Fixation with Layered Bismuth Oxyhalides, *Acc. Chem. Res.*, 2017, **50**(1), 112–121.

21 H. Li, J. Shang, Z. H. Ai and L. Z. Zhang, Efficient Visible Light Nitrogen Fixation with BiOBr Nanosheets of Oxygen Vacancies on the Exposed {001} Facets, *J. Am. Chem. Soc.*, 2015, **137**(19), 6393–6399.

22 Y. Liu, X. Kong, X. Guo, Q. Li, J. Ke, R. Wang, Q. Li, Z. Geng and J. J. A. C. Zeng, Enhanced N_2 electroreduction over $LaCoO_3$ by introducing oxygen vacancies, *ACS Catal.*, 2020, **10**(2), 1077–1085.

23 R. Jia, Y. Wang, C. Wang, Y. Ling, Y. Yu and B. J. A. C. Zhang, Boosting selective nitrate electroreduction to ammonium by constructing oxygen vacancies in TiO_2, *ACS Catal.*, 2020, **10**(6), 3533–3540.

24 B. He, Y. Cao, K. Lin, Y. Wang, Z. Li, Y. Yang, Y. Zhao and X. Liu, Strong Interactions between Au Nanoparticles and $BiVO_4$ Photoanode Boosts Hole Extraction for Photoelectrochemical Water Splitting, *Angew. Chem., Int. Ed.*, 2024, **63**(23), e202402435.

25 C. Ma, H. Zhang, J. Xia, X. Zhu, K. Qu, F. Feng, S. Han, C. He, X. Ma, G. Lin, W. Cao, X. Meng, L. Zhu, Y. Yu, A.-L. Wang and Q. Lu, Screening of Intermetallic Compounds Based on Intermediate Adsorption Equilibrium for Electrocatalytic

Nitrate Reduction to Ammonia, *J. Am. Chem. Soc.*, 2024, **146**(29), 20069–20079.

26 V. I. Merupo, S. Velumani, G. Oza, M. Tabellout, M. Bizarro, S. Coste and A. H. Kassiba, High Energy Ball-Milling Synthesis of Nanostructured Ag-Doped and $BiVO_4$-Based Photocatalysts, *ChemistrySelect*, 2016, **1**(6), 1278–1286.

27 X. J. Yu, S. J. Du, Z. Z. Xu, J. He, F. Z. Liu, B. Wang, S. D. Sun, Y. F. Tang and K. Zhao, Surface-enhanced bimetallic effect of Au-Pd by internal electromagnetic fields from $Au@Cu_2O$ for efficient electrochemical nitrate reduction to ammonia, *Chem. Eng. J.*, 2024, **480**, 148152.

28 A. E. ElMetwally, M. S. Sayed, J. J. Shim, M. R. Knecht and L. G. Bachas, Plasmon-Enhanced Photocatalytic Oxidation of Benzyl Alcohol to Benzaldehyde Using $BiVO_4$/BiOBr/Au Nanosheets, *ACS Appl. Nano Mater.*, 2023, **6**(7), 5909–5917.

29 W. Zhang, T. Y. Wang, X. J. Xing, H. H. Yin, J. Li, W. Xiong and H. Li, Effects of Surfactants on the Size Distribution and Electrocatalytic Nitrite Reduction of Uniformly Dispersed Au Nanoparticles, *ACS Sustain. Chem. Eng.*, 2024, **12**(28), 10313–10324.

30 M. Yuan, J. Chen, Y. Bai, Z. Liu, J. Zhang, T. Zhao, Q. Wang, S. Li, H. He and G. Zhang, Unveiling Electrochemical Urea Synthesis by Co-Activation of CO_2 and N_2 with Mott-Schottky Heterostructure Catalysts, *Angew. Chem., Int. Ed.*, 2021, **60**(19), 10910–10918.

31 N. A. R. Che Mohamad, K. Chae, H. Lee, J. Kim, F. Marques Mota, J. Bang and D. H. Kim, Synergistic effect of oxygen vacancies and in-situ formed bismuth metal centers on $BiVO_4$ as an enhanced bifunctional $Li–O_2$ batteries electrocatalyst, *J. Colloid Interface Sci.*, 2025, **678**, 119–129.

32 R. Su, M. He, N. Li, D. Ma, W. Zhou, B. Gao, Q. Yue and Q. Li, Visible-Light Photocatalytic Chlorite Activation Mediated by Oxygen Vacancy Abundant Nd-Doped $BiVO_4$ for Efficient Chlorine Dioxide Generation and Pollutant Degradation, *ACS Appl. Mater. Interfaces*, 2022, **14**(28), 31920–31932.

33 M. L. Yuan, J. W. Chen, Y. L. Bai, Z. J. Liu, J. X. Zhang, T. K. Zhao, Q. N. Shi, S. W. Li, X. Wang and G. J. Zhang, Electrochemical C-N coupling with perovskite hybrids toward efficient urea synthesis, *Chem. Sci.*, 2021, **12**(17), 6048–6058.

34 H. Li, F. Qin, Z. Yang, X. Cui, J. Wang and L. Zhang, New Reaction Pathway Induced by Plasmon for Selective Benzyl Alcohol Oxidation on BiOCl Possessing Oxygen Vacancies, *J. Am. Chem. Soc.*, 2017, **139**(9), 3513–3521.

35 X. Li, Z. Wang, A. Sasani, A. Baktash, K. Wang, H. Lu, J. You, P. Chen, P. Chen, Y. Bao, S. Zhang, G. Liu and L. Wang, Oxygen vacancy induced defect dipoles in $BiVO_4$ for photoelectrocatalytic partial oxidation of methane, *Nat. Commun.*, 2024, **15**(1), 9127.

36 W.-J. Sun, L.-X. Li, H.-Y. Zhang, J.-H. He and J.-M. Lu, A Bioinspired Iron-Centered Electrocatalyst for Selective Catalytic Reduction of Nitrate to Ammonia, *ACS Sustain. Chem. Eng.*, 2022, **10**(18), 5958–5965.

37 Y. Wang, W. Yu, X. Li, J. Yu and W. Zhou, Electrocatalytic reduction of nitrogenous pollutants to ammonia, *Chem. Eng. J.*, 2023, **469**, 143889.